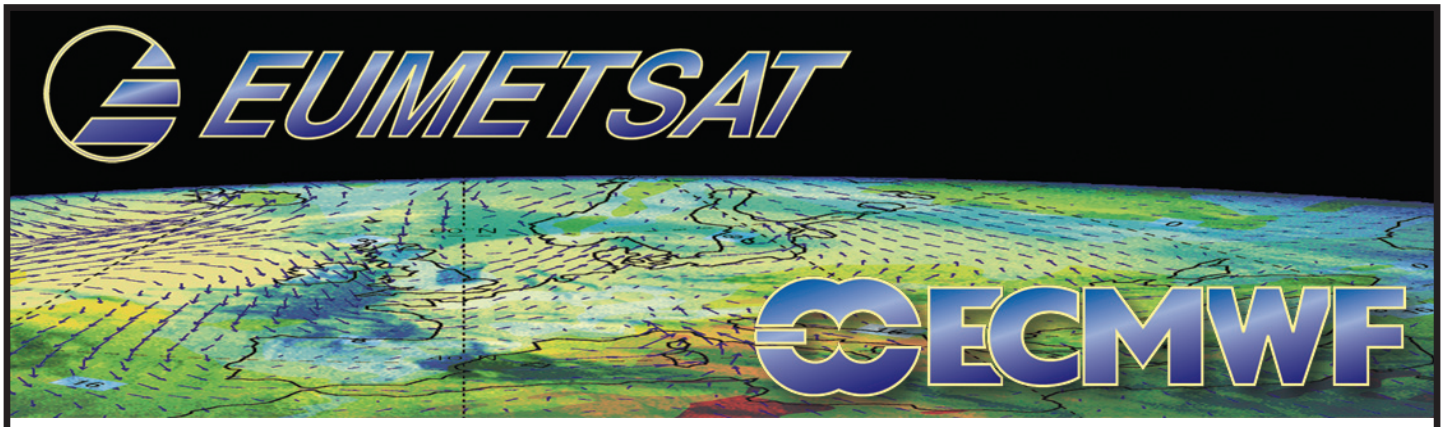


EUMETSAT/ECMWF Fellowship Programme
Research Report No. 19

# Revision of the HIRS cloud detection at ECMWF

B. Krzeminski, N. Bormann, G. Kelly, T. McNally and P. Bauer

October 2009

Series: EUMETSAT/ECMWF Fellowship Programme Research Reports

A full list of ECMWF Publications can be found on our web site under:
http://www.ecmwf.int/publications/

Contact: library@ecmwf.int



European Centre for Medium Range Weather Forecasts
Shinfield Park, Reading, RG2 9AX, England

**Abstract**

HIRS radiances are assimilated routinely at ECMWF. Assimilation of clear-sky radiances requires cloud-contaminated observations to be identified and rejected. The old operational cloud detection procedure was found to leave residual cloud contamination in the assimilated scenes.

In this document, we describe the recent revision of the HIRS cloud detection procedure. The HIRS cloud detection scheme aims at finding clear-sky channels within each field of view. It exploits the differences (fg-departures) between observed radiances and their simulated first guess clear-sky counterparts and inter-channel gradients. Selected HIRS scenes were analysed to understand the cause of undetected cloud contamination. It was found that noise in the fg-departures often masked the presence of a cloud or was misinterpreted as a cloud signature. Smoothing was introduced to the fg-departures to reduce the noise. Thresholds used in the cloud detection have also been revised.

The revised cloud detection is shown to detect cloud contamination more reliably, more consistent with the results from the IASI cloud detection. Departure histograms after cloud screening are more symmetric and comparisons with MSG imagery suggest that the revised algorithm detects clouds more reliably. Forecast experiments did not show statistically significant impact of the revision on the forecast accuracy. The revised cloud detection scheme was applied operationally from cycle 35r2.

# 1 Introduction

The HIRS instrument provides measurements of the atmospheric state in twelve longwave infrared channels (channels 1–12 from 14.96 μm to 6.74 μm), seven shortwave infrared channels (channels 13–19 from 4.57 μm to 4.46 μm) and one visible channel (channel 20 at 0.69 μm). Channels 1–15 are either assimilated or passively monitored at ECMWF (over ocean and sea ice, channels being assimilated are 4,5,6,7,11,12,14 and 15; over land, only channel 12 is assimilated). Three HIRS instruments are currently in use at ECMWF: HIRS/3 onboard NOAA-17, HIRS/4 on METOP-A and recently introduced NOAA-19.

HIRS measurements are assimilated in clear-sky conditions only and provide information about temperature (longwave channels 4,5,6,7,14 and 15) and water vapour (shortwave channels 11 and 12). Prior to the assimilation, cloud-contaminated observations must be identified and rejected.

The HIRS cloud detection scheme aims at finding clear-sky channels within each field of view. To do so, the channels are considered in the order of increasing pressures at the peak of the weighting function, and the first channel is identified that shows considerable cloud contamination. The channels with weighting function peaks above this channel are deemed cloud-free. We summarise here results of a recent revision of the scheme to improve its performance and simplify the implementation.

In the old approach, two screening tests were used and data was rejected if one of the two tests indicated clouds. The first method was based on threshold tests applied to the first guess departures (fg-departures) of the window channel 8. Channel $i$ was flagged clear-sky if

$$min_{ij} < \Delta BT_8 < max_{ij} \tag{1}$$

where

$$\begin{aligned} &i \in \{1,2,\ldots,8,10,\ldots,15\} \\ &j \in \{\text{S.Polar, S.MidLat, Tropical, N.MidLat, N.Polar}\} \end{aligned} \tag{2}$$

Here, $\Delta BT_8$ is the window channel 8 fg-departure and $min_{ij}$, $max_{ij}$ are the thresholds that depend on the channel number $i$ and latitude region $j$ (Table 1). This test was implemented as an elaborate set of IFS blacklisting rules.

In the second algorithm (Kelly, 2007) the presence of the cloud signature was tested by applying thresholds to the differences ("gradients") of normalized fg-departures and to the fg-departures themselves. The algorithm considered channels 3–8 where channel 3 peaks around the tropopause and other channels peak progressively lower in the atmosphere. A cloud signature in channel $i$ was identified either if

$$\left| \frac{\Delta BT_i}{\sigma_i} - \frac{\Delta BT_{i-1}}{\sigma_{i-1}} \right| > 1.5 \tag{3}$$

or

$$|\Delta BT_i| > 3\sigma_i \tag{4}$$

where $i$ iterates from 3 to 8, $\Delta BT_i$ is the fg-departure for the $i$-th channel and $\sigma_i$ is the expected standard deviation of the clear-sky fg-departures of the $i$-th channel (Table 2). These standard deviations were pre-computed from a carefully selected set of clear-sky fg-departures, as described in Kelly (2007).

Tests 3 and 4 will be called together "old gradient check" hereafter for brevity. The gradient check is applied only to the longwave $CO_2$ band channels 3–8. When the cloud signature is found in the $i$-th channel, channels $i, i+1, \ldots, 8$ are rejected as cloud contaminated. Stratospheric channels 1 and 2 are assumed to be always clear. For the shortwave channels 9–15, each one is screened by applying the result of a gradient check of a corresponding longwave channel. The correspondence between shortwave and longwave channels is shown in Table 3. The HIRS gradient check is similar to the algorithm developed for the IASI cloud screening (McNally and Watts, 2003).

The described cloud detection procedure has been revised as the monitoring of the recently introduced METOP-A HIRS/4 instrument at ECMWF suggested that the data, after cloud screening, still had some residual cloud contamination, particularly in channels 5 and 6 (Bormann and Thépaut, 2007). A secondary goal of the revision was to simplify the scheme by removing the elaborate blacklist cloud checks and using the gradient check alone.

In the following, we summarize the results of the revision of the HIRS cloud detection, as implemented operationally on 10 March 2009.

| | thresholds (K) by latitude region | | | | | | | | | |
|---|---|---|---|---|---|---|---|---|---|---|
| | [90°S, 60°S] | | (60°S, 30°S] | | (30°S, 30°N] | | (30°N, 60°N] | | (60°N, 90°N] | |
| channel | min | max | min | max | min | max | min | max | min | max |
| 1 | -40.0 | 40.0 | -40.0 | 40.0 | -40.0 | 40.0 | -40.0 | 40.0 | -40.0 | 40.0 |
| 2 | -40.0 | 40.0 | -40.0 | 40.0 | -40.0 | 40.0 | -40.0 | 40.0 | -40.0 | 40.0 |
| 3 | -40.0 | 40.0 | -40.0 | 40.0 | -40.0 | 40.0 | -40.0 | 40.0 | -40.0 | 40.0 |
| 4 | -12.0 | 12.0 | -10.0 | 10.0 | -5.0 | 5.0 | -8.0 | 8.0 | -8.0 | 8.0 |
| 5 | -6.0 | 6.0 | -4.0 | 4.0 | -2.0 | 3.0 | -4.0 | 4.0 | -4.0 | 4.0 |
| 6 | -6.0 | 6.0 | -4.0 | 4.0 | -2.0 | 3.0 | -4.0 | 4.0 | -4.0 | 4.0 |
| 7 | -1.0 | 2.0 | -1.0 | 2.0 | -1.0 | 2.0 | -1.0 | 2.0 | -1.0 | 2.0 |
| 8 | -1.0 | 2.0 | -1.0 | 2.0 | -1.0 | 2.0 | -1.0 | 2.0 | -1.0 | 2.0 |
| 10 | -1.5 | 3.0 | -1.5 | 3.0 | -1.5 | 3.0 | -1.5 | 3.0 | -1.5 | 3.0 |
| 11 | -2.0 | 4.0 | -2.0 | 4.0 | -2.0 | 4.0 | -2.0 | 4.0 | -2.0 | 4.0 |
| 12 | -10.0 | 10.0 | -10.0 | 10.0 | -10.0 | 10.0 | -10.0 | 10.0 | -10.0 | 10.0 |
| 13 | -1.8 | 3.0 | -1.5 | 3.0 | -1.2 | 3.0 | -1.5 | 3.0 | -1.8 | 3.0 |
| 14 | -3.0 | 3.0 | -2.5 | 3.0 | -1.6 | 3.0 | -2.0 | 3.0 | -2.5 | 3.0 |
| 15 | -4.0 | 4.0 | -3.0 | 3.0 | -2.0 | 3.0 | -3.0 | 3.0 | -3.0 | 3.0 |

*Table 1: Thresholds of the old HIRS blacklist cloud detection*

# 2 Revision of the cloud detection algorithm

## 2.1 Method

The first step of the HIRS cloud detection revision was to disable the blacklist check and analyse the performance of the gradient check working alone. The histogram on Figure 1a shows the result of disabling the blacklist check for the fg-departures of HIRS channel 6 used data. An increased amount of negative fg-departures suggests that the gradient test alone failed to identify a significant number of cloud contaminated observations. Figure 1b further suggests that the blacklist test was much more effective in the old cloud detection procedure than the gradient test. Figure 2 supports this conclusion.

In a first attempt to improve the performance of the gradient test, normalization coefficients $\sigma_i$ in Equation 3 and 4 were recalculated and a threshold used in Equation 3 was retuned. However, merely retuning these parameters was not successful, as reliable cloud detection could only be achieved at the expense of excessive rejection of (frequently clear-sky) data. To understand these difficulties, many individual scenes were analysed. Figure 3 illustrates an example case. The gradient test detected a cloud signature in channel 5 for apparently clear-sky conditions (case "B" in the Figure). The fg-departure plot further illustrates the false cloud signature (possibly noise amplified by the normalization). Also, over the warm ocean surface, cloud contamination should give negative fg-departure gradients. In the example, a positive gradient was classified as a cloud signature.

| channel | old scheme $\sigma$ (K) | new scheme $\sigma$ (K) |
|---|---|---|
| 2 | 0.25 | — |
| 3 | 0.26 | 0.423 |
| 4 | 0.26 | 0.214 |
| 5 | 0.29 | 0.213 |
| 6 | 0.38 | 0.283 |
| 7 | 0.50 | 0.415 |
| 8 | 0.84 | 0.685 |

*Table 2: Estimations of standard deviations ($\sigma$) of HIRS clear-sky fg-departures; $3\sigma$ values are used as thresholds in the HIRS cloud detection scheme; in the old version of the algorithm they were also used as normalization coefficients for the fg-departures.*

| channel | sensitivity | QC channels old | QC channels new |
|---|---|---|---|
| 9 | ozone | 8 | 7 |
| 10 | low level water vapour | 8 | 8 |
| 11 | mid level water vapour | 7 | 7 |
| 12 | mid level water vapour | 5 | 5 |
| 13 | low level temperature | 8 | 8 |
| 14 | low level tropospheric temperature | 7 | 7 |
| 15 | middle level tropospheric temperature | 6 | 7 |

*Table 3: HIRS channels 9-15 and their corresponding longwave channels used for cloud screening.*

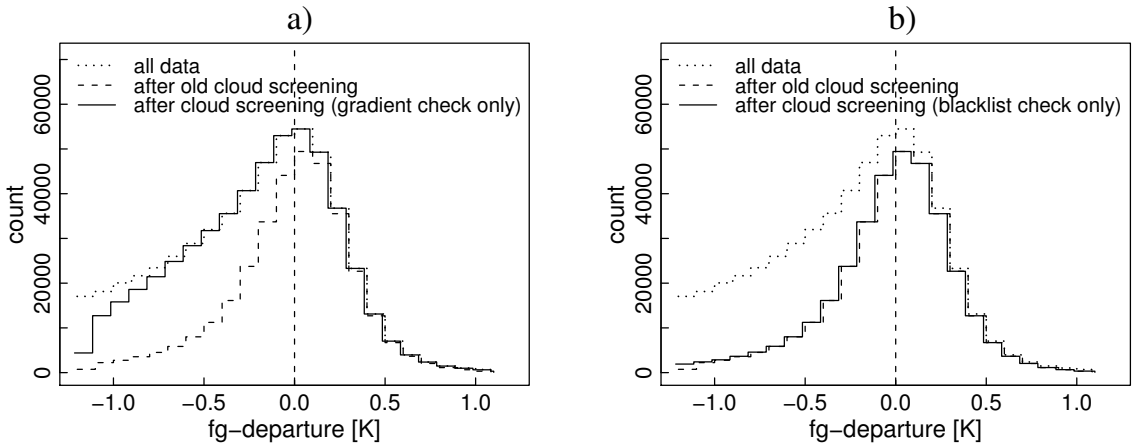


*Figure 1: Effect of removing the blacklist test (a) or the gradient test (b) from the old operational HIRS cloud detection scheme on the population of channel 6 fg-departures flagged as clear-sky; populations for all-sky fg-departures and data after the full cloud detection are also shown for comparison; bin size is 0.1K; 3 days of global METOP-A HIRS/4 data (2008.12.17 - 2008.12.19) over ocean were used to calculate the statistics.*

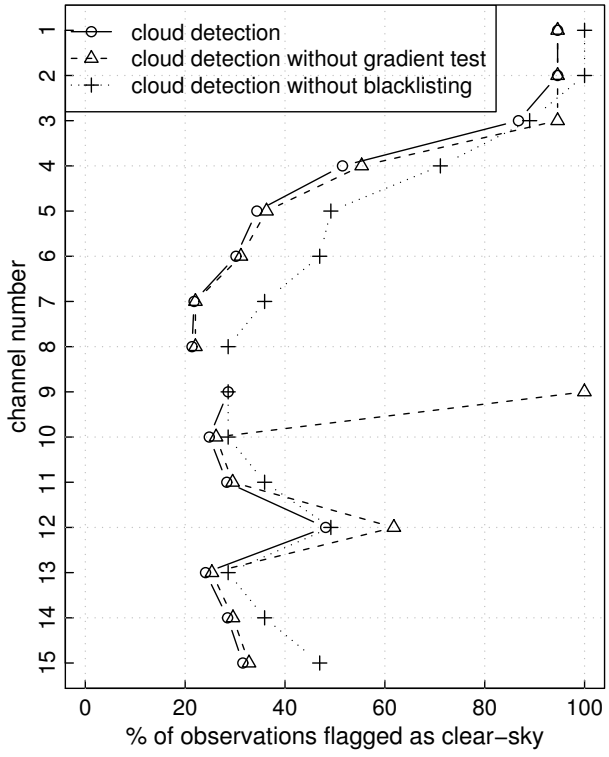


*Figure 2: Effect of removing the gradient test ($\triangle$) or the blacklist test ($+$) from the old operational HIRS cloud detection scheme ($\circ$) on the proportion of data flagged as clear-sky. 24 hours of global METOP-A HIRS data were used to calculate the statistics.*

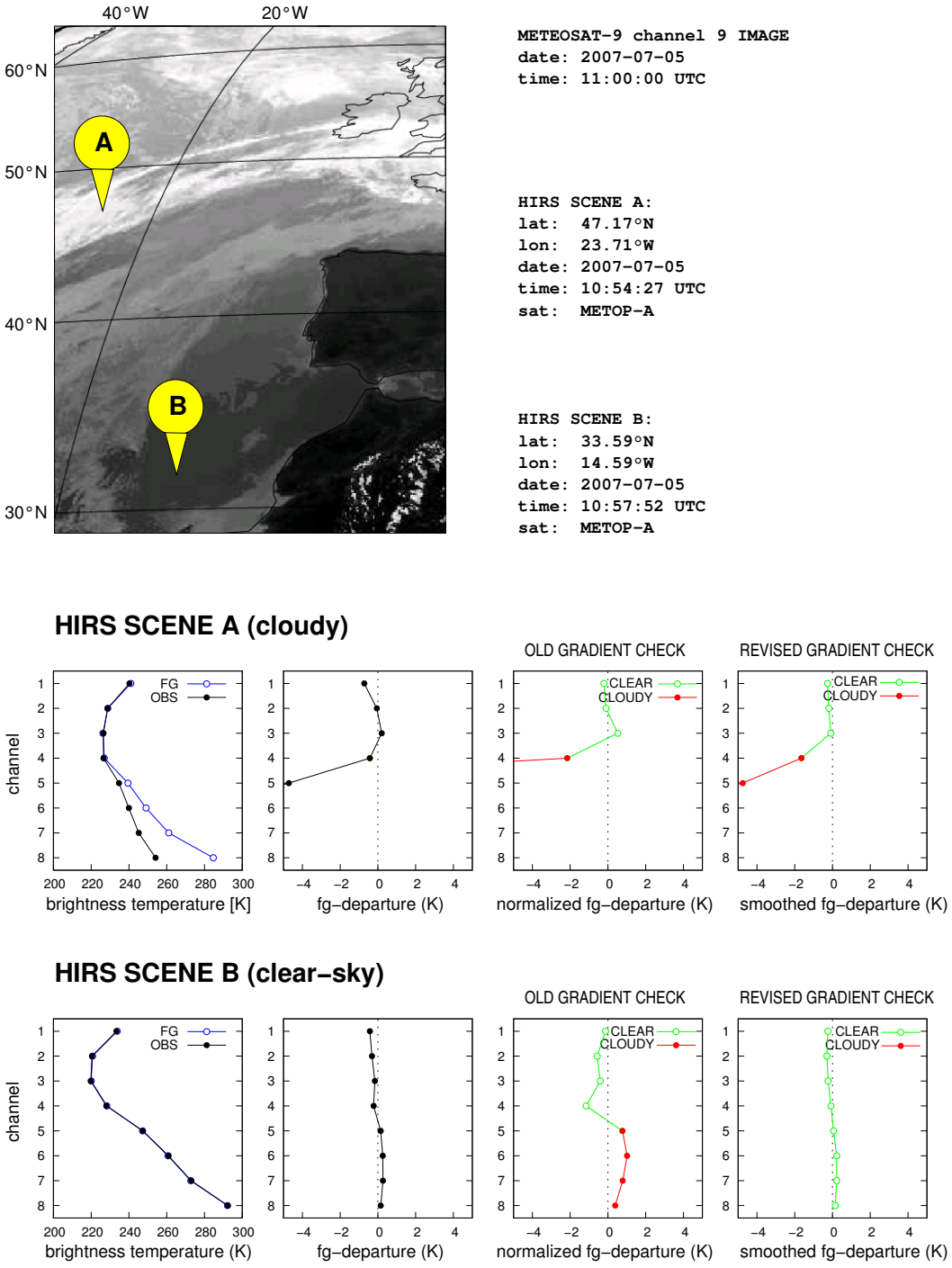


*Figure 3: Illustration of the HIRS gradient check performance for two example scenes (clear and cloudy); in case B, the old gradient check detected a false cloud signature in channel 5, and the revised algorithm version correctly identified the scene as clear-sky. See main text for more details.*

| channel pair | threshold (K) |
|---|---|
| 3–2 | 0.22 |
| 4–3 | 0.22 |
| 5–4 | 0.12 |
| 6–5 | 0.25 |
| 7–6 | 0.23 |
| 8–7 | 0.30 |

*Table 4: Thresholds used in the revised gradient test; these are applied to the differences of smoothed fg-departures of two channels.*

Based on these findings, the gradient algorithm was modified. For each scene being checked, smoothing is now applied to the fg-departures as a preliminary step:

$$\Delta BT_i^{'} = \begin{cases} \frac{1}{3}\Delta BT_{i-1} + \frac{1}{3}\Delta BT_i + \frac{1}{3}\Delta BT_{i+1} & \text{for } i = 3,4,5,6,7 \\ \Delta BT_i & \text{for } i = 8 \end{cases} \tag{5}$$

where $i$ is the channel number and $\Delta BT_i^{'}$ is the smoothed fg-departure. Next, the threshold tests are applied to the differences of the smoothed fg-departures rather than the normalized fg-departures as in the old scheme. Previously a single threshold (1.5) was used in the gradient check (Formula 3). The revised scheme uses different thresholds for different channel pairs (table 4).

A cloud signature in channel $i$ is found if any of the conditions (6) (7) is true:

$$\Delta BT_i^{'} - \Delta BT_{i-1}^{'} > r_i \tag{6}$$

$$\left|\Delta BT_i^{'}\right| > 3\sigma_i \tag{7}$$

where $r_i$ is the threshold used for checking the $i$-th channel for the cloud signature and $\sigma_i$ are the recalculated estimations of the clear-sky fg-departues. Channel number $i$ iterates from 3 to 8 (the iteration stops if the cloud signature is found). Finally, when the cloud signature is found in channel $i$ by one of the above checks, an additional check is applied to confirm the cloud signature - the next gradient must be at least 80% of the current gradient or the signature will be considered false. The cloud signature found in channel $i$ is confirmed if

$$\Delta BT_{i+1}^{'} - \Delta BT_i^{'} > 0.8(\Delta BT_i^{'} - \Delta BT_{i-1}^{'}) \tag{8}$$

where $i$ is the channel number for which the cloud signature was found. The confirmation test is applicable for $i = 3,4,\ldots,7$.

For the scenes with a cloud warmer than the surface, the differences in Formula 6 are expected to be negative and tests 6 and 8 are modified: inequality signs are reversed and a negative threshold is used in 6. The cases where modified tests 6 and 8 should be used are determined by checking if the following two conditions are both true:

$$T_{surface} < 274K \tag{9}$$

$$\Delta BT_8^{'} - \Delta BT_4^{'} > 0.5 \tag{10}$$

Such scenes are typically found at high latitudes, particulary during the winter, and are believed to be associated with the temperature profile inversions. Figure 4 shows an example locations of these cases for two different times of the year.

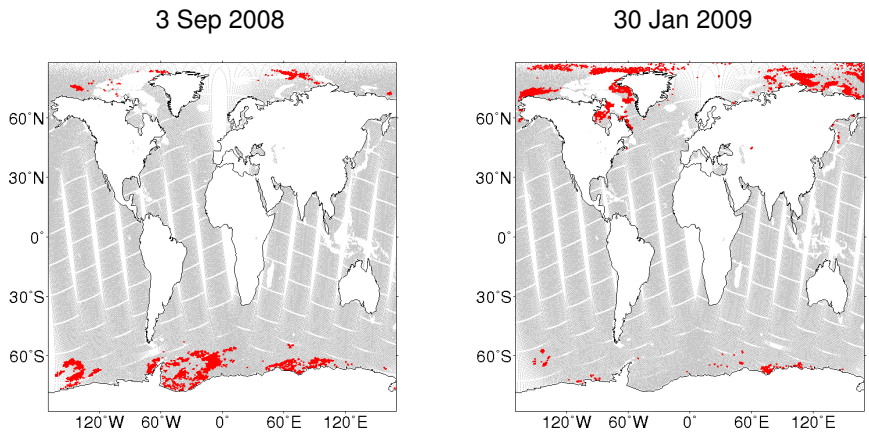


*Figure 4: Scenes classified by the revised HIRS cloud detection scheme as possibly contaminated by a warm cloud over cold surface (red); each plot shows 12 hours of METOP-A HIRS coverage.*

The initial estimations of the $\sigma_i$ were obtained from the carefully selected set of clear-sky fg-departures, as described in Kelly (2007). However, these were later modified in the process of retuning the scheme. Values for $r_i$ were obtained empirically, using the fg-departure histogram shapes as a guidance in the retuning process. $r_i$ were retuned starting from $i = 3$, then proceeding to $i = 4$ and so on. This way, retuning of the $i$-th threshold did not change the results of the cloud detection for already retuned channels.

The screening of the shortwave channels based on the correspondence between shortwave and longwave channels was also revised (see Table 3). It was necessary as the new gradient check for channels 1–8 resulted in an asymmetric fg-departure histogram for cloud screened channel 15 fg-departures (not shown), suggesting that a residual cloud contamination is present. In the revised scheme, channel 15 is linked with channel 7 instead of the higher peaking channel 6, resulting in more symmetric channel 15 fg-departure histogram. For channel 9, it was found that channel 7 could be used instead of the window channel 8 without significant change in the channel 9 fg-departure histograms. Note that channel 9 is not used in the operational assimilation of HIRS data.

## 2.2 Interaction with VarBC

Note that check 6 is asymmetric (for example for the cold cloud over warm surface, only negative fg-departure gradients are rejected). It is known that asymmetric quality control can cause unwanted feedback between the quality control and the adaptive bias correction (Auligné and McNally, 2007). In early trials, such feedback was indeed observed for channel 8. Bias coefficients of ECMWF's variational bias correction scheme exhibited significant drift for the two month test period. Also, the number of channel 8 data diagnosed as clear was gradually decreasing. No such effects were observed in the control experiment. From histogram plots (Fig.5) it was evident that the bias of channel 8 fg-departures had been increasing as the experiment progressed (Fig.5a) causing the quality control to reject more and more data (Fig.5b). Biased channel 8 fg-departures also introduced a negative bias in channel 7 smoothed fg-departures and more cases of negative gradients for channel pair 6–7. These gradients were then interpreted as cloud signatures. Indeed, the number of used data quality data for channel 7 had a decreasing trend, similar to channel 8.

An additional modification was therefore made to the gradient check to eliminate the described effects. For channel 8, asymmetric check 6 was replaced with a symmetric check. A cloud signature is found in channel 8

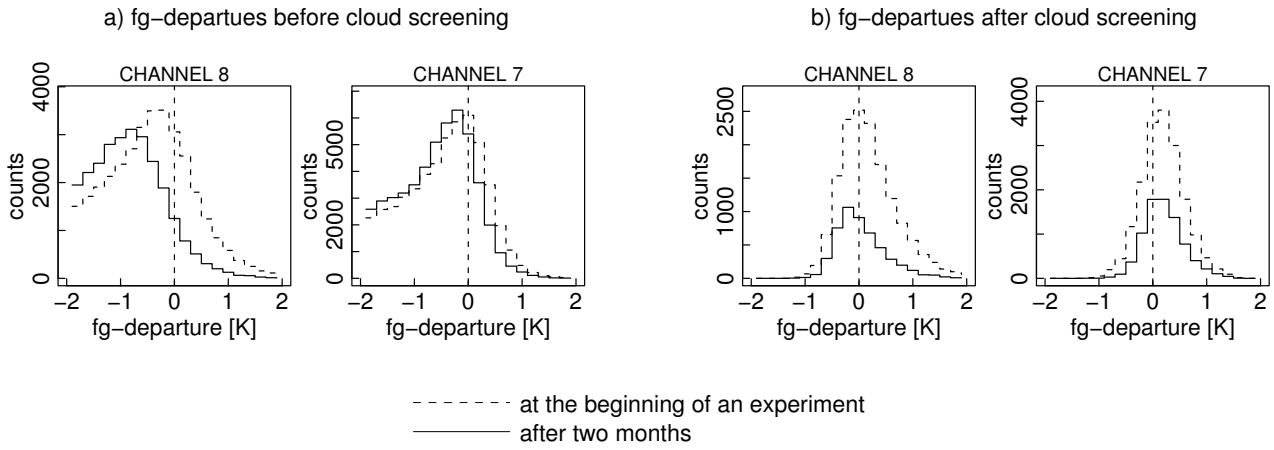


*Figure 5: Interaction between METOP-A HIRS bias correction and the cloud screening as shown in histograms of fg-departures for channel 8 and 7 for all data (a) and cloud-screened data (b). The asymmetric quality control test caused a bias increase in channel 8 as the experiment progressed (a); the cloud screening responded by rejecting more data in channels 8 and 7 (b)*

if

$$\left|\Delta BT_8^{'} - \Delta BT_7^{'}\right| > r_8 \tag{11}$$

This modification succesfully avoided the drifts in the bias correction noted above. It is worth pointing out that the asymmetric approach as formulated in 6 is physically more sensible, and the symmetric check is only introduced to stabilize the variational bias correction. In the future, it may be possible to avoid the observed drift by using the mode of the fg-departure as norm in the variational bias correction (Han and McNally, 2008).

## 2.3 Performance

The effect of the revised cloud detection on the statistics of the quality controlled data is shown in Figure 6. The number of negative fg-departures was reduced in channels 5, 6 and 7 leading to more symmetric histograms, which suggests the revised cloud detection works more reliably compared to the old scheme.

The HIRS cloud detection is similar to the IASI cloud detection as both aim to find clear channels within each observed scene. The presence of both instruments on board METOP-A allowed a straightforward comparison of the performance of their cloud screening results. HIRS-equivalent IASI channels were selected on the basis of similar weighting functions. These were calculated using the RTTOV-7 software for the U.S.Standard Atmosphere profiles. To verify the accuracy of the channel matching, the correlation between observed brightness temperatures for collocated HIRS and IASI observations was checked. Figure 7 shows scatterplots of observed brightness temperatures for HIRS channels against selected IASI channels. Generally these plots confirm the accuracy of the channel matching based on weighting functions. Only HIRS channels 1 and 4 show some discrepancies with IASI channels, but no better equivalents could be found among the subset of IASI channels used at ECMWF (Collard, 2007).

The proportion of data flagged as clear-sky by the revised cloud detection before and after thinning is shown in Figure 8. For reference, this is compared to the results of the old HIRS scheme and also to the IASI cloud detection. It can be seen that the number of data passing the revised cloud test is reduced, compared to the old scheme, bringing the fraction of clear-sky observations closer to that detected by the IASI algorithm.

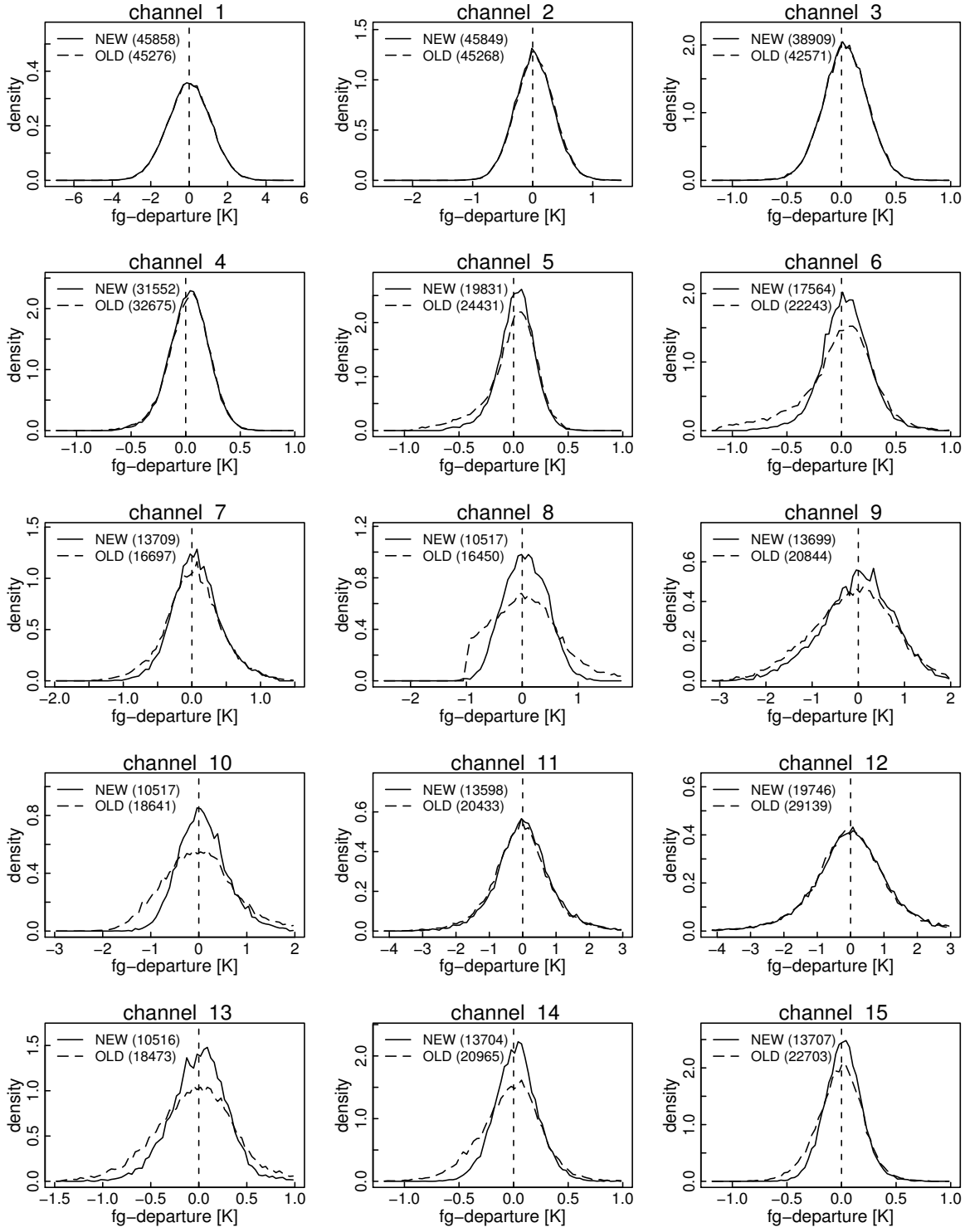


*Figure 6: METOP-A HIRS/4 fg-departure density plots after bias correction, cloud screening and thinning for the old (dashed line) and revised (solid line) cloud detection scheme; two days of global HIRS/4 data over ocean (2009.01.29–2009.01.30) were used to calculate the statistics.*

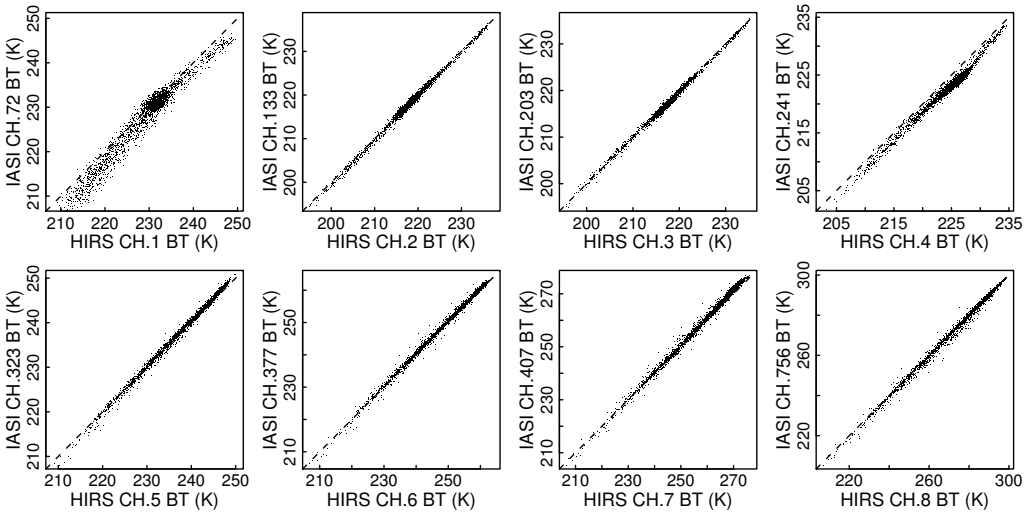


*Figure 7: Scatterplots of HIRS against collocated "HIRS equivalent" IASI channels. 12 hours of global METOP-A HIRS and IASI data was used.*

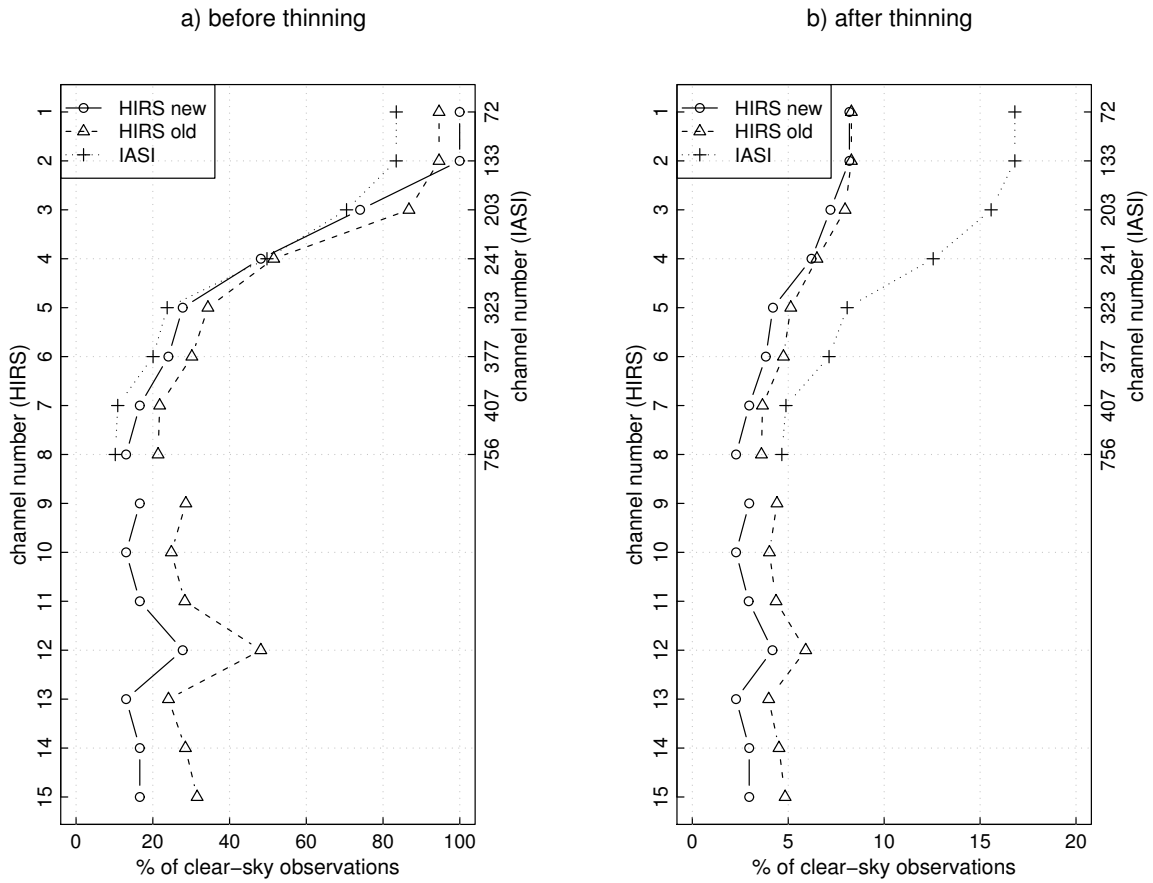


*Figure 8: Proportion of observations flagged as clear-sky by the old (△) and revised (○) cloud detection algorithms for HIRS; the IASI operational cloud screening (+) is also shown for reference. Left panel shows proportions after the cloud screening but before thinning. Right panel shows proportions for thinned data. 24 hours of METOP-A HIRS/4 and IASI data (2008.12.19) were used to calculate the proportions.*

Figure 9 shows an example coverage of the METOP-A HIRS/4 and METOP-A IASI clear-sky data in selected channels on top of the METEOSAT near infrared image. The revised scheme seems to reliably distinguish between clear-sky and cloudy regions. It now performs very similar to the IASI cloud detection, as can be seen from the good consistency between the areas considered as clear in the two scenes in Figure 3.

Results of the revised HIRS cloud screening at higher latitudes were verified against MODIS cloud top pressure product (Menzel et al., 2008). Figure 10 shows an example comparison for the case near the South Pole.

The impact of the revised HIRS cloud detection scheme on the forecast scores was neutral. It was tested in a forecast experiment consisting of 61 forecast cases, covering November and September 2007. IFS version CY32R3 was used. The horizontal and vertical model resolution was T255 (≈80km) and L91 respectively with analysis increments calculated at T159 (≈125km).

Figure 11 shows the normalized differences between RMS errors of the geopotential forecasts of the control experiment and an experiment with the revised HIRS cloud detection scheme. The new cloud detection has no statistically significant impact on the geopotential forecasts, within the 90% confidence level. Similar neutral impact was observed for other prognostic variables.

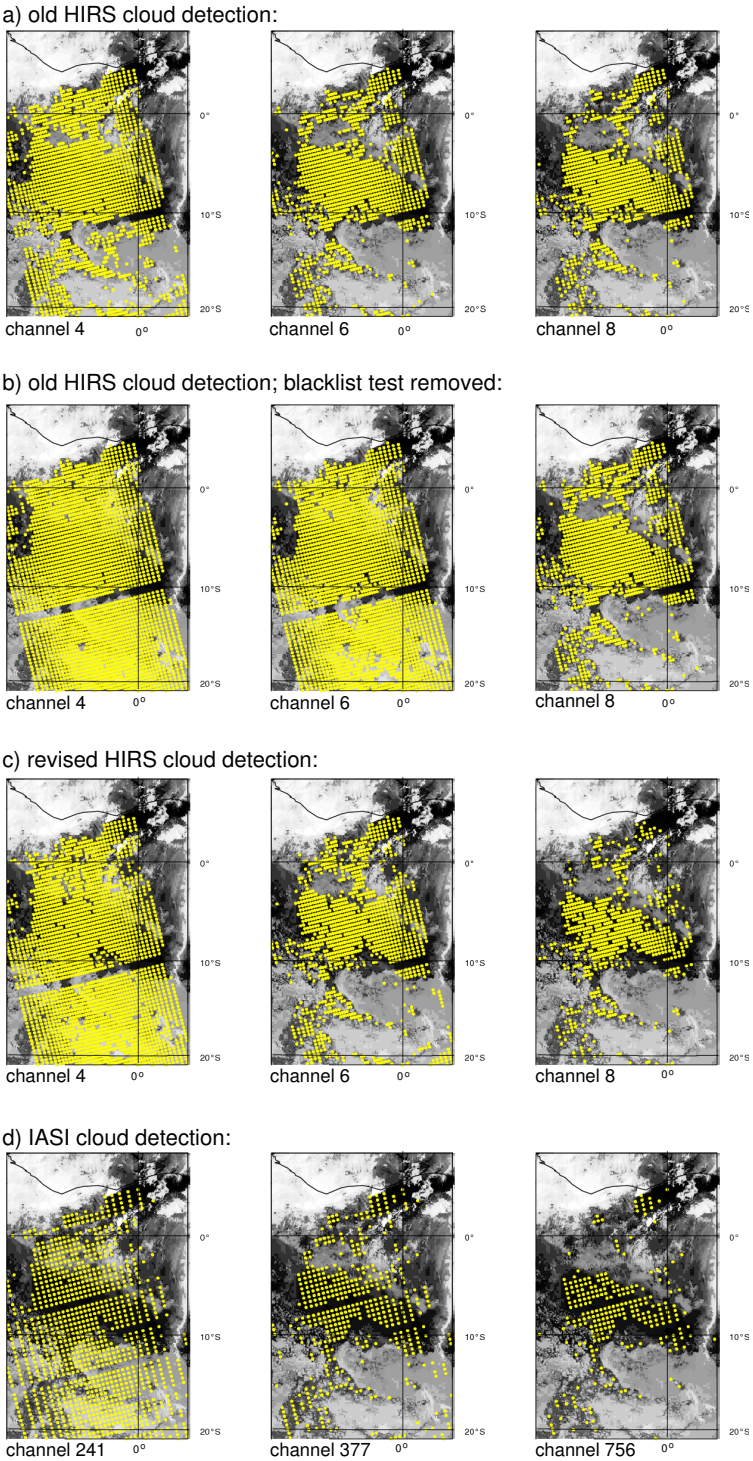


*Figure 9: An example of METOP-A HIRS/4 coverage for selected channels after the cloud screening. IASI coverage is also shown for reference; date and time: 18 December 2008 around 22:00 UTC; background image: METEOSAT-9 channel 9 (10.8* μm*).*

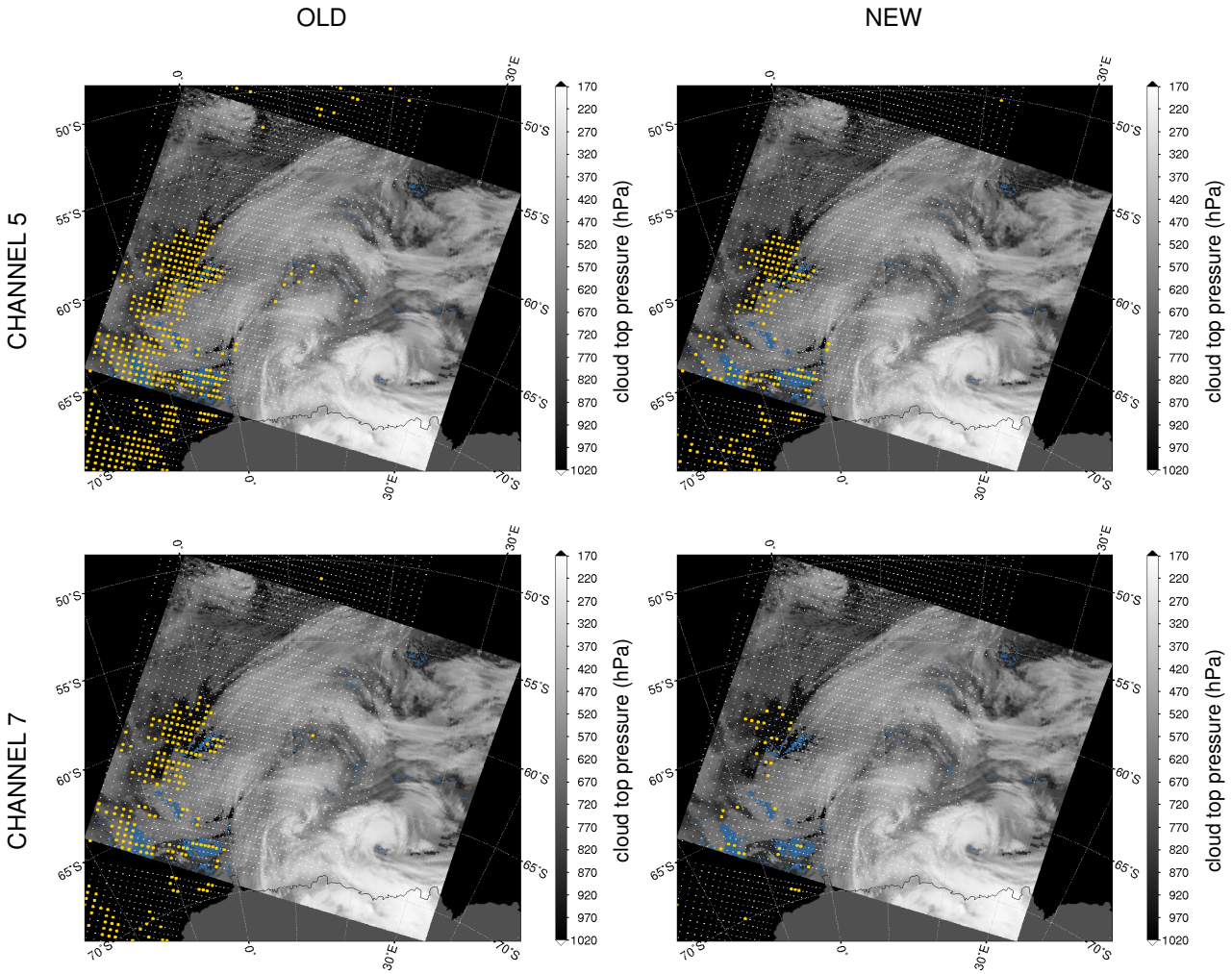


*Figure 10: Cloud-free METOP-A HIRS observations (yellow dots) for two selected channels overlaid on the map of cloud top pressure retrieved from TERRA MODIS. Old HIRS cloud detection algorithm is demonstrated on the left, new one on the right; date and time of the MODIS granule: 2008-09-02 08:40 UTC*

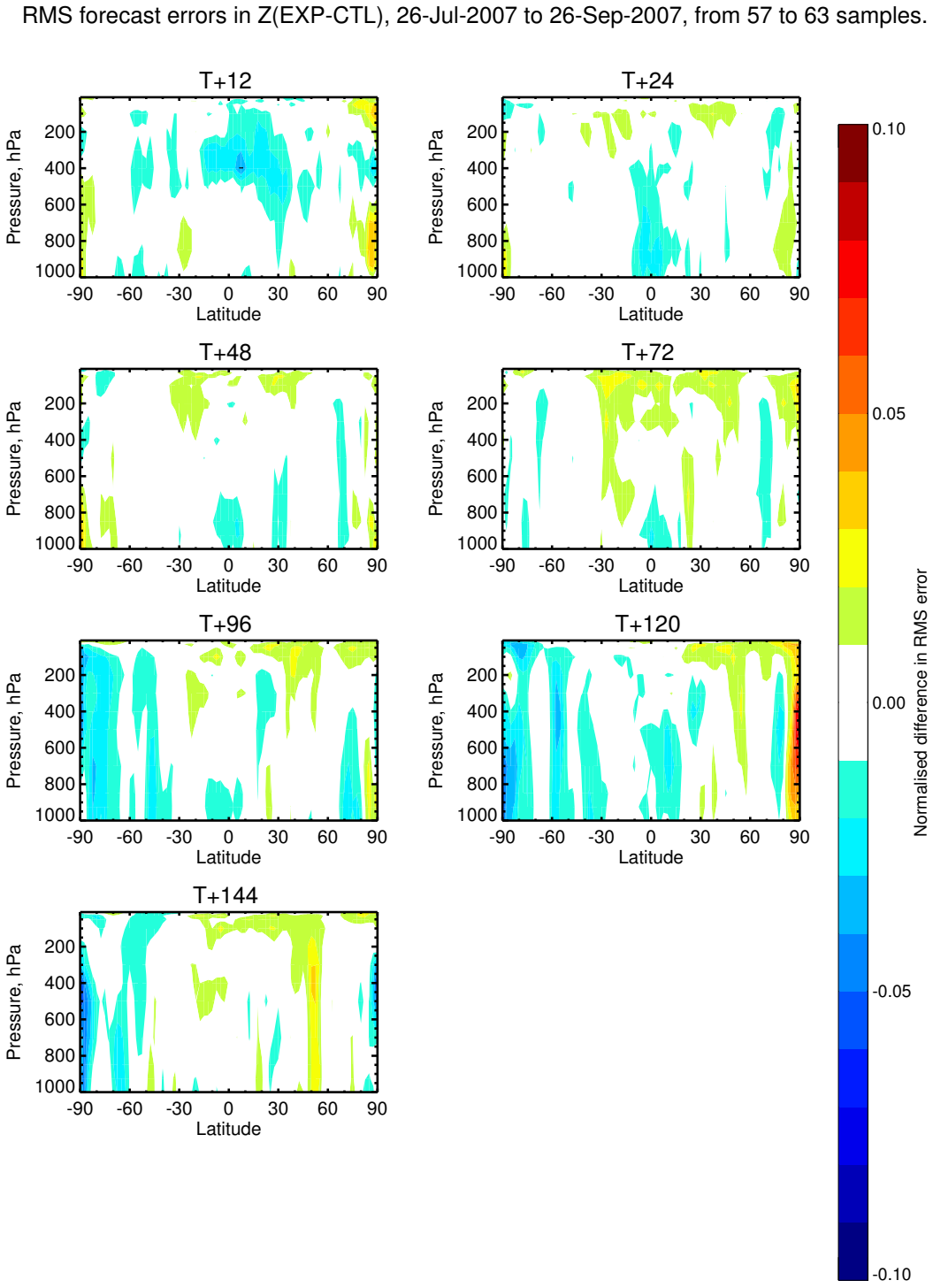


*Figure 11: Neutral impact of the revised HIRS cloud detection on the RMS forecast errors; zonal means of normalized differences between RMS forecast errors (experiment minus control) for the geopotential are shown; blue areas correspond to the improvement in the forecast accuracy (statistically significant differences would be distinguished as cross-hatched regions).*

# 3 Summary

The HIRS cloud detection scheme has been revised to improve its reliability in detecting cloud contaminated observations and simplify the implementation. The revised scheme was shown to distinguish clear and cloudy observations with greater accuracy, mainly as a result of applying a smoothing algorithm to the fg-departures. The revised cloud detection shows an improved consistency with the IASI cloud detection. The implementation of the revised cloud detection was simplified by removing now redundant blacklist cloud checks. The impact of the new cloud detection on the forecast skill appears to be neutral.

The revised scheme has been introduced into ECMWF's operational analysis system on 10 March 2009 as part of the 35r2 cycle of the IFS library.

Due to the reliance of the scheme on the fg-departures, it may be necessary to retune cloud detection gradient thresholds for the Reanalysis project.

# 4 Acknowledgements

The authors thank Andrew Collard for providing jacobians of IASI and HIRS channels and Alan Geer for the forecast verification software. Blazej Krzeminski was funded by the EUMETSAT Fellowship programme.

# References

Auligné, T. and A. McNally (2007). Interaction between bias correction and quality control. *Q.J.R.Meteorol.Soc. 133*, 643–653.

Bormann, N. and J.-N. Thépaut (2007). Use of HIRS from METOP. ECMWF research department memorandum, ECMWF.

Collard, A. D. (2007). Selection of IASI channels for use in numerical weather prediction. *Quarterly Journal of the Royal Meteorological Society 133*, 1977–1991.

Han, W. and A. McNally (2008). Bias correction of window channels on microwave and infrared sounders. NWP-SAF Visiting Scientist report, ECMWF.

Kelly, G. (2007). The evaluation of the HIRS/4 instrument on METOP 2 by using the ECMWF data assimilation system to provide a reference to compare with other sensors. Technical Memorandum 523, ECMWF.

McNally, A. P. and P. Watts (2003). A cloud detection algorithm for high-spectral-resolution infrared sounders. *Quarterly Journal of the Royal Meteorological Society 129*, 3411–3423.

Menzel, W. P., R. A. Frey, H. Zhang, D. P. Wylie, C. C. Moeller, R. E. Holz, B. Maddux, B. A. Baum, K. I. Strabala, and L. E. Gumley (2008). MODIS global cloud-top pressure and amount estimation: Algorithm description and results. *Journal of Applied Meteorology and Climatology 47*, 1175–1198.